THE JOURNAL OF PHYSICAL CHEMISTRY C

ARTICLE

pubs.acs.org/JPCC

Conversion of [0001] Textured ZnO Nanofilm into [01$\bar{1}$0] Directed Nanowires Driven by CO Adsorption: In Situ Carbothermal Synthesis and Complementary First Principles Thermodynamics Simulations

Paresh Shimpi, Satyesh Kumar Yadav, Ramamurthy Ramprasad,* and Pu-Xian Gao*

Department of Chemical, Materials and Biomolecular Engineering and Institute of Material Science, University of Connecticut, Storrs, Connecticut 06269-3136, United States

Supporting Information

ABSTRACT: An in situ carbothermal process has been utilized to successfully convert sputtered (0001) oriented ZnO nanofilm into large scale [01$\bar{1}$0] directed nanowires at 800−900 °C in a tubular reaction chamber. To understand the conversion process and unravel the driving force behind this growth phenomenon, a comparative study has been carried out on the thermal annealing processes of ZnO nanofilms under different gas flows (with or without Ar flow) and atmosphere (with or without graphite source input) controls. It is found that the graphite source and Ar flow are both necessary to induce the conversion of ZnO (0001) oriented nanofilm into ZnO nanowires grown along [01$\bar{1}$0]. By heating the graphite source, a C- or CO-rich reducing atmosphere was generated and carried downstream by Ar flow during the conversion process, which proved to be the key. Complementary first principles computations suggest that changes in the ordering of surface energies in the presence of CO occur. As compared with the clean facets with an order of {10$\bar{1}$0}, {11$\bar{2}$0}, and {0001} from most to least stable, upon CO adsorption at high temperatures (900 °C), the {11$\bar{2}$0} and {0001} surfaces become more stable as compared to {10$\bar{1}$0}. This provides a strong thermodynamic driving force for the growth of nanowires along ⟨10$\bar{1}$0⟩ directions.

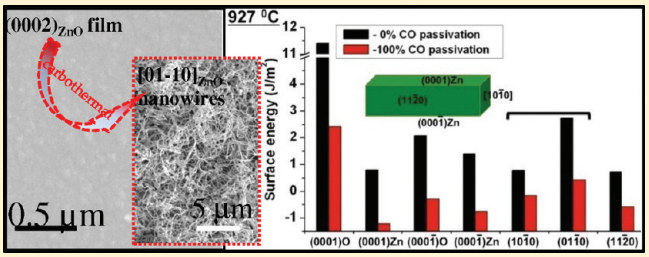

Extensive research effort has been paid toward the large scale synthesis of uniformly distributed functional nanowires.[1−3] This is driven by the need of mass production of nanomaterials, so-called "nanomanufacturing", before the possible commercialization in their applications for constructing ultrasensitive nanosensors,[4,5] high performance solar cells,[6,7] low threshold field emitters, and many others. The realization of nanomanufacturing demands novel but simple approaches with the rational and precise control over structure and morphology of nanomaterials, which, however, is still lacking understanding, hindering the manufacturing of various nanomaterials. For example, various types of ZnO nanostructures such as nanobelts, nanowires, and nanotubes can be routinely fabricated under different conditions,[8−18] but why it can happen in different ways is far from well understood. Using a carbothermal vapor transport method, ZnO nanotubes,[19] nanowires,[20] and nanobelts[21] can be achieved, respectively, at relatively low, middle, and high temperature ranges. It is believed that the evaporation process involving prepumping level, pressure, growth time as well as temperature plays a key role to introduce different morphological nanostructures. However, microscopically and thermodynamically why various nanostructure growth phenomena can occur remains unclear in this carbothermal vapor transport process. On the other hand, as a nanostructure conversion process, the carbothermal vapor transport method is also recognized to usually leave a large amount of reacted precursors without conversion into the desired nanostructures.

In this work, using a simple in situ carbothermal method, [0001] textured ZnO nanofilm was successfully converted into large scale nanowires with a growth direction along ⟨01$\bar{1}$0⟩ at ∼800−900 °C. A comparative experimental and theoretical study has been carried out to understand this conversion process. To start with, ∼3 g of graphite powder (Fisher Scientific) loaded in an alumina boat was used as the source material and kept in the tube furnace center, as shown in the Figure 1a. Silicon substrate sputtered with 50 nm ZnO nanofilms was placed ∼10 cm away from the source. During the experiment, the furnace was heated to 1200 °C with a ramping rate of 25 °C/min and kept for 2 h. The pressure was controlled at ∼100 mbar when the temperature reached 1000 °C, and carrier gas Ar was initiated at 20 sccm. During the cooling period, Ar gas was stopped when the temperature reached 1000 °C. Figure 1b shows the schematic of the final result where sputtered ZnO nanofilm (50 nm) converted into uniformly distributed ZnO nanowires with a very high yield at a temperature range of ∼800−900 °C. A JEOL JSM

Received: February 10, 2011
Revised: March 13, 2011
Published: March 31, 2011

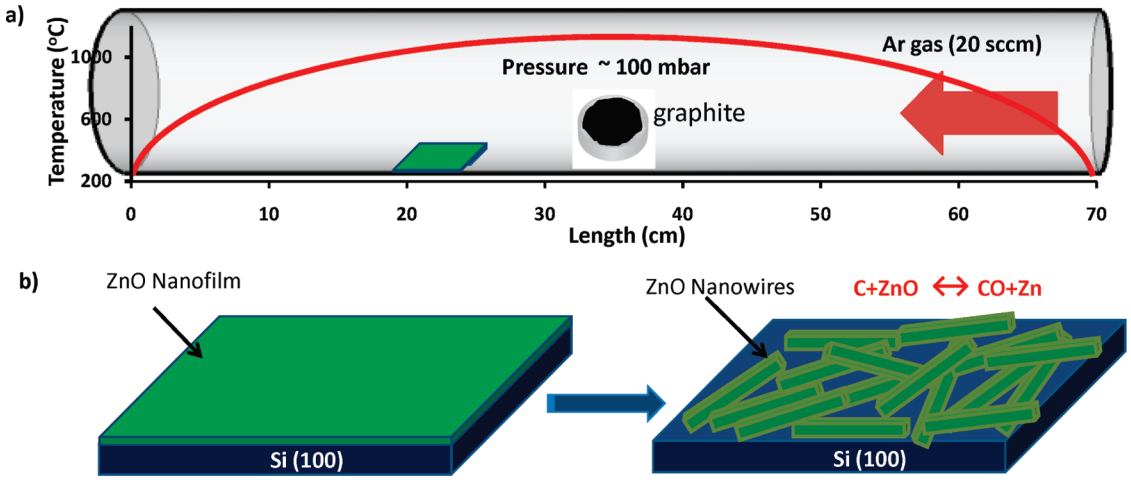

Figure 1. (a) Schematic diagram of the in situ carbothermal ZnO nanowires growth setup. (b) Schematic diagram of in situ ZnO nanofilm (i) conversion into ZnO nanowires and (ii) in the presence of appropriate gas flow.

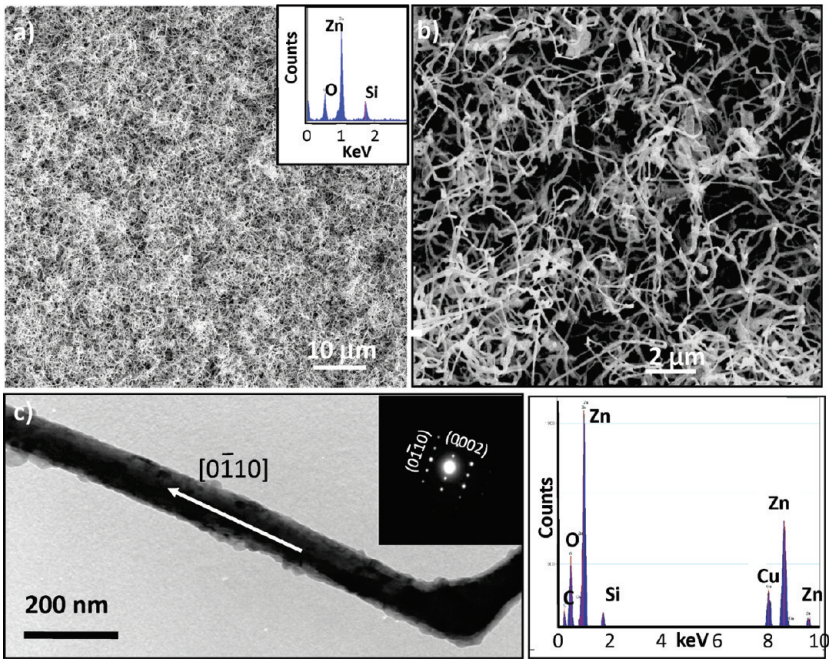

Figure 2. (a) Typical low magnification SEM image of zigzag ZnO nanowires. Inset in (a): the EDX spectrum of ZnO nanowires, (b) a high magnification SEM image of zigzag ZnO nanowires, (c) a representative TEM image of ZnO nanowire and the corresponding selected area electron diffraction (SAED) pattern (inset in c), and (d) a typical EDX spectrum of single nanowire in TEM.

6335F field emission scanning electron microscope (SEM) and an FEI Tecnai 12 scanning transmission electron microscope (STEM) were used to characterize the morphology and structure of the converted nanowires. The composition was determined by energy dispersive X-ray (EDX) spectrometers attached to the SEM and TEM.

Figure 2a is a top-view SEM image of large scale as-converted zigzag ZnO nanowire, and the inset displays the EDX spectrum revealing the presence of Zn, O, and Si. A silicon peak appears due to the Si substrate. Figure 2b is a high magnification SEM image of the converted ZnO nanowires ~100 nm wide and a few micrometers long. A typical TEM image of zigzag ZnO nanowires and the corresponding selective area electron diffraction (SAED) pattern in Figure 2c reveal the single crystalline wurtzite structured nanowire grown along the $[01\bar{1}0]$ direction. Figure 2d is an EDX spectrum of a single nanowire confirming the composition of ZnO nanowire, while the copper peak is due to the TEM Cu grid. Here, sputtered ZnO nanofilm has a (0001) orientation as proved by the X-ray diffraction pattern shown in Figure 3a, which is energetically more favorable than $(11\bar{2}0)$ and $(01\bar{1}0)$. The zigzag nature of ZnO nanowires grown along $[01\bar{1}0]$ is consistent with an early report, which suggested that the zigzag structure of single crystal nanowires results from the periodic change in equivalent growth directions of $\langle 01\bar{1}0\rangle$, that is, from $[1\bar{1}00] \rightarrow [10\bar{1}0] \rightarrow [01\bar{1}0] \rightarrow [10\bar{1}0]$.[22]

To investigate the conversion process of [0001] oriented ZnO nanofilm into $[01\bar{1}0]$ nanowires, a series of comparative experiments have been designed and conducted, as listed in Table 1.

dx.doi.org/10.1021/jp201320d |J. Phys. Chem. C 2011, 115, 7372–7376

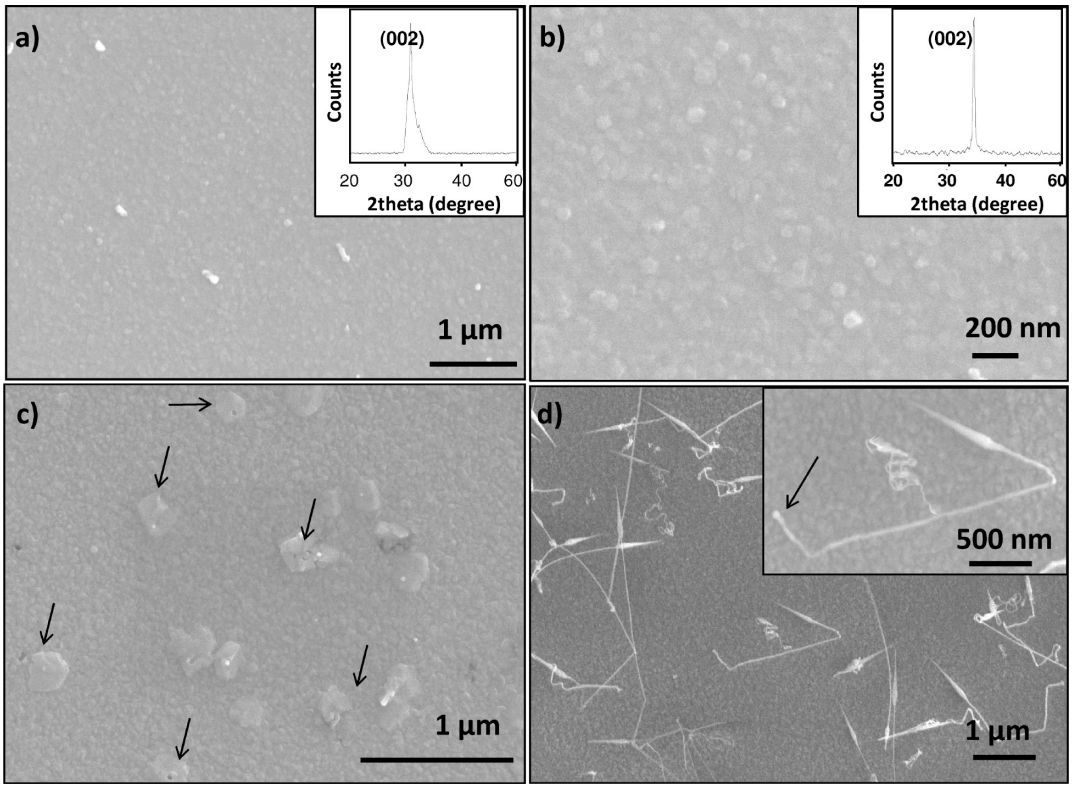

Figure 3. (a) Typical SEM image of ZnO sputtered silicon substrate after 1 h of annealing at ~800−900 °C in the absence of graphite as a source and Ar as a carrier gas (inset: the corresponding XRD pattern of 50 nm ZnO nanofilm on silicon substrate after annealing), (b) a high magnification SEM image revealing nanoisland formation, (c) a typical SEM image of sputtered ZnO nanofilm annealed at ~800−900 °C for 1 h in presence of graphite as a source and Ar as a carrier gas, and (d) ZnO nanowires grown from the nanoislands after a prolonged (1.5 h) annealing at at ~800−900 °C in the presence of Ar and graphite (inset of d: a zoom-in SEM image showing a ZnO nanowire grown from a nanoisland).

Table 1. Different Experimental Conditions for In Situ Thermal Annealing of (0001)-Oriented ZnO Nanofilms

furnace center temperature (°C)	duration (min)	Ar flow (20 sccm)	graphite (C)	result
1200	60	absent	absent	tiny nanoislands (Figure 3a)
1200	60	present	present	large nanoislands (Figure 3c)
1200	90	present	present	nanowires with a low (~10%) yield (Figure 3d)
1200	120	present	present	nanowires with a high (~90%) yield (Figure 2a,b)

The involvement of graphite source and Ar flow simultaneously has been suggested to be necessary through the experiment observations and rational comparison. On the 50 nm ZnO nanofilm coated Si, after thermal annealing at ~800−900 °C for 1 h in the absence of graphite and carrier gas, 20−50 nm ZnO nanoislands formed quite uniformly (Figure 3a,b). The inset X-ray diffraction pattern in Figure 3b reveals that the textured (001) orientation of nanoisland-based ZnO film was intact after thermal annealing. It is clear that the high temperature annealing process transforms the as-sputtered ZnO nanofilms from smooth and flat surfaces consisting of fine nanoparticles to rough surfaces filled with coarsened nanoislands.[23] As a comparison, upon annealing for 1 h at ~800−900 °C, with Ar as a carrier gas and graphite as a source (Figure 3c), the ZnO nanoisland size further increased, and some nanoislands grew bigger as compared to others as a result of the coarsening effect. This coarsening phenomenon is due to a natural self-organization of the surface adatoms driven by the reduction of surface area, therefore, surface energy. With the input of the graphite source and Ar carrier gas flow, another hour and a half of thermal annealing clearly brings up the nucleation and growth of nanowires, as evidenced in Figure 3d. These nanowires are 2−10 μm in length and less than 100 nm in diameter. The inset picture in Figure 3d clearly shows that nanowires grew from the nanoisland as indicated by arrowheads. This result suggests that as the temperature increases, the nanofilm first breaks down into the nanoislands[24,25] (Figure 3c). With a further increase of temperature, nanorods or nanowires formed, with the pass-by gas flow (carbon + Ar) potentially providing the transient reduction and in situ recombination of comprised atoms in the deposited compound (Zn−O in our case), which therefore could favor the formation of nanowires.[26,27]

It is well-known that preferred growth directions of nanostructures are determined by surface energies. Any factors that could change the magnitude and ordering of the surface energies of various surface facets of a system may be expected to alter the preferred growth directions. Such a phenomenon has been recently predicted for CdSe nanocrystals[28] and subsequently verified experimentally.[29]

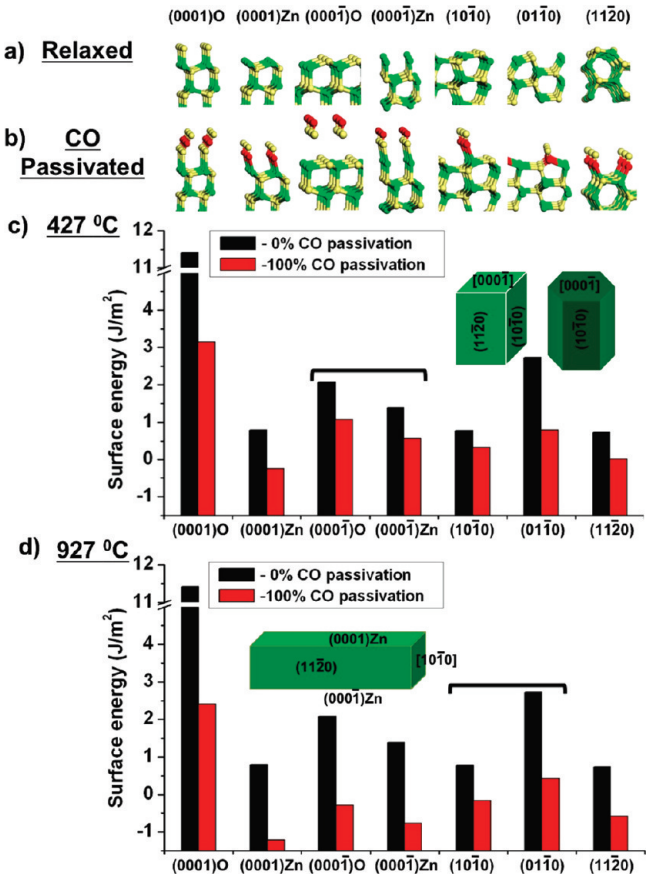

Figure 4. (a) Relaxed geometries of the polar (0001)O, (0001)Zn, (000$\bar{1}$)O, and (000$\bar{1}$)Zn and nonpolar (10$\bar{1}$0), (01$\bar{1}$0), and (11$\bar{2}$0) facets of ZnO. (b) The corresponding relaxed surface configuration after stoichiometric binding with CO (O, Zn, and C atoms are shown in yellow, green, and red, respectively). (c) Calculated surface free energies of the facets before and after CO passivation at 427 °C. (d) The corresponding surface free energy results at 927 °C. In parts c and d, surfaces with normals along the preferred growth directions are bracketed, and the insets show nanowire schematics indicating nanowire growth direction (high surface energy) and enclosing surfaces (low surface energy).

While in the absence of O, no particular growth direction is favored in the case of CdSe, and the presence and adsorption of O stabilizes all surface facets (including the (000$\bar{1}$) facets) except the (0001) surfaces. Thus, O adsorption allows preferential anisotropic and asymmetric growth along the [0001] direction. Likewise, it is plausible that the unusual ⟨01$\bar{1}$0⟩ growth directions seen experimentally in the case of ZnO nanowires may be due to the stabilization of all surface facets except the {01$\bar{1}$0} surfaces mediated by CO adsorption.

To completely understand the role of CO in determining facet stability order, a density functional theory (DFT) study combined with statistical thermodynamics was performed. The surface free energies of various crystal facets were computed in the presence and absence of adsorbed CO at various temperatures, including the nonpolar (11$\bar{2}$0), (10$\bar{1}$0), and (01$\bar{1}$0) surfaces and the polar (0001) and (000$\bar{1}$) facets. We make the important observation that the polar facets are not equivalent and come in four surface configurations. The Zn- versus O-terminated (0001) facets contain surface atoms with one and three dangling bonds, respectively, and are referred to henceforth as (0001)Zn and (0001)O. Similarly, the Zn- and O-terminated (000$\bar{1}$) facets are decorated with surface atoms that display three and one dangling bonds, respectively, and are represented as (000$\bar{1}$)Zn and (000$\bar{1}$)O. Figure 4a illustrates the surface configurations of all polar and nonpolar facets considered. Further details concerning the theory and simulations are provided in the Materials and Methods section of the Supporting Information.

A few comments concerning the tendency of surfaces to relax to their ground state configurations are in order. As discussed extensively before,[28] one may take recourse to basic electron and bond counting rules to understand the relaxation patterns of various surface facets. In the case of the nonpolar facets, electrons from dangling bonds at surface Zn atoms are redistributed to surface O atoms. This results in surface Zn atoms having no dangling bonds (i.e., approaching an sp^2-like configuration), while each surface O atom retains an sp^3-like configuration because of its lone pair of electrons. The sp^2-like configuration results in a planar structure as opposed to the sp^3-like tetrahedral configuration, which is apparent in the relaxed nonpolar surfaces of Figure 4a. On the other hand, in the case of the polar facets, where Zn or O atoms exhibit either one or three dangling bonds, there is no clear pathway for such surface relaxation. Thus, the polar facets undergo negligible relaxation.

On nonpolar facets, CO prefers to adsorb on a surface Zn atom via the C atom forming the σ bond, although the binding energy for CO binding via the O atom is only slightly higher.[30] On the (0001)Zn polar facet, CO binds via the C atom forming the σ bond, while on (000$\bar{1}$)Zn, the binding is via the O atom thus forming next layer of the crystal along [000$\bar{1}$] direction. Figure 4b shows the binding mode and configurations of CO covered polar and nonpolar facets.

We next move on to our surface free energy calculations. These computations explicitly included the vibrational contribution to the free energy due to CO adsorbates on the surfaces (thus, temperature dependence is appropriate only for CO covered surfaces). Moreover, we have assumed that the surfaces are covered by a monolayer of CO. Figure 4c shows a comparison of the surface free energies in the absence and presence of CO at 427 °C. It can be seen that CO adsorption results in a substantial decrease in surface energy of the highly unstable (0001)O surface, while the surface energy of other facets undergoes smaller decreases. Nevertheless, the ordering of the surface energies is preserved. Figure 4d shows an analogous set of results but at a higher temperature of 927 °C. Further small reductions in the magnitude of the surface energies, but more importantly, changes in the ordering of the surface energies can be seen.

To determine the preferred growth direction based on these results, we need to consider the following. For growth to occur along a certain direction, all facets and not just one that would get successively created during growth along that direction should be of high surface energy. For instance, for vigorous growth to occur preferentially along the [0001] direction, the surface energy of both the (0001)Zn and the (0001)O surfaces should necessarily be high relative to that of all other surface facets. Likewise, for growth to occur along the [000$\bar{1}$] direction, both (000$\bar{1}$)Zn and (000$\bar{1}$)O facets have to display high surface energies. Among the nonpolar surfaces, (10$\bar{1}$0) and (01$\bar{1}$0) facets have their normals along the same direction, and for growth to occur along this direction, both these surfaces have to display higher surface energies as compared to other enclosing crystal facets. Along the [11$\bar{2}$0] direction, only one type of surface forms successively. The results presented in Figure 4 are ordered so that related

dx.doi.org/10.1021/jp201320d |J. Phys. Chem. C 2011, 115, 7372–7376

surfaces appear adjacent to each other. On the basis of the above considerations for preferred growth, it can be concluded from Figure 4 that at low temperatures (and in the absence of CO), growth is preferred along the $[000\bar{1}]$ direction (consistent with prior work at 427 °C[31,32]), but at high temperatures, the preferred growth direction switches to $[10\bar{1}0]$. These conclusions are indicated by square brackets in Figure 4c,d, and the insets show the possible nanowire configurations consistent with our conclusions.

To be precise, in the presence of graphite and carrier gas, sputtered ZnO nanofilm turns into nanoislands at higher temperature, which is further converted into nanowire. With increasing time and temperature, under CO-rich conditions, $\{11\bar{2}0\}$ and $\{0001\}$ surfaces are more stable as compared to $\{10\bar{1}0\}$ surfaces, thus favoring nanowire growth along $\langle 10\bar{1}0\rangle$ direction.

In summary, an in situ carbothermal process has been utilized to successfully convert sputtered (0001) oriented ZnO nanofilm into large scale nonpolar $[01\bar{1}0]$ directed nanowires at ~800−900 °C, clearly with a larger surface area being generated. To understand the counterintuitive conversion process and the driving force behind this growth phenomenon, a comparative study has been carried out on the thermal annealing processes of ZnO nanofilm under different gas flows (with or without Ar flow) and atmosphere (with or without graphite source input) controls. It is found that the graphite source and Ar flow both are necessary parameters to induce the conversion of ZnO (0001) oriented nanofilm into ZnO nonpolar nanowires directly. By heating the graphite source, a C- or CO-rich reducing atmosphere has been generated and carried by Ar flow for this conversion process, which proved to be the key. Complementary first principles computations suggest that the changes in the ordering of surface energies in the presence of CO occur. As compared with the clean surfaces with an order of $\{10\bar{1}0\}$, $\{11\bar{2}0\}$, and $\{0001\}$ from most to least stable, upon CO adsorption at high temperatures (900 °C), the $\{11\bar{2}0\}$ and $\{0001\}$ surfaces become more stable as compared to $\{10\bar{1}0\}$. This gives a strong thermodynamic driving force for the growth of nanowires in $\langle 10\bar{1}0\rangle$ directions. This work may provide important physical and chemical insights for helping understand, design, and rationally synthesize nanostructures with different surface configurations toward nanomanufacturing.

■ ASSOCIATED CONTENT

Supporting Information. Methods and models, figure of surface free energies for the polar and nonpolar surfaces of ZnO at four different temperatures, and references. This material is available free of charge via the Internet at http://pubs.acs.org.

■ AUTHOR INFORMATION

Corresponding Author

*E-mail: rampi@ims.uconn.edu (R.R.) or puxian.gao@ims.uconn.edu (P.-X.G.).

■ ACKNOWLEDGMENT

We thank the financial support from the University of Connecticut New Faculty start-up funds, the University of Connecticut large faculty research grant, the Department of Energy, and the CBET Division of the National Science Foundation. Acknowledgement is also made to the Donors of the American Chemical Society Petroleum Research Fund for partial support of this research.

■ REFERENCES

(1) Xia, Y.; Yang, P.; Sun, Y.; Wu, Y.; Mayer, B.; Gates, B.; Yin, Y.; Kim, F.; Yan, H. *Adv. Mater.* **2003**, *15* (5), 353–389.
(2) Whang, D.; Jin, S.; Wu, Y.; Lieber, C. M. *Nano Lett.* **2003**, *3* (9), 1255–1259.
(3) Greene, L. E.; Law, M.; Goldberger, J.; Kim, F.; Johnson, J. C.; Zhang, Y.; Saykally, R. J.; Yang, P. *Angew. Chem., Int. Ed.* **2003**, *42*, 3031–3034.
(4) Cui, Y.; Qingqiao, W.; Park, H.; Lieber, C. M. *Science* **2001**, *293* (5533), 1289–1292.
(5) Wang, Z. L. *J. Phys.: Condens. Matter* **2004**, *16*, R829–R858.
(6) Law, M.; Greene, L. E.; Johnson, J. C.; Saykally, R.; Yang, P. *Nat. Mater.* **2005**, *4*, 455–459.
(7) Baxter, J. B.; Aydil, E. S. *App. Phys. Lett.* **2005**, *86*, 053114(1)–53114(3).
(8) Yu, S.-H.; Liu, B.; Mo, M.-S.; Huang, J.-H.; Liu, X.-M.; Qian, Y.-T. *Adv. Funct. Mater.* **2003**, *13* (8), 639–647.
(9) Wang, Z.; Liu, J.; Chen, X.; Wan, J.; Qian, Y. *Chem.—Eur. J.* **2005**, *11*, 160–163.
(10) Vayssieres, L. *Adv. Mater.* **2003**, *15*, 464–466.
(11) Shimpi, P.; Gao, P. X.; Gobermann, D.; Ding, Y. *Nanotechnology* **2009**, *20*, 125608–125615.
(12) Lee, W.; Jeong, M.-C.; Myoung, J.-M. *Nanotechnology* **2004**, *15*, 254–259.
(13) Bao, X.-Y.; Soci, C.; Susac, D.; Bratvold, J.; Alpin, D. P. R.; Wei, W.; Chen, C.-Y.; Dayeh, S. A.; Kavanagh, K. L.; Wang, D. *Nano Lett.* **2008**, *8* (11), 3755–3760.
(14) Gao, P. X.; Wang, Z. L. *J. Phys. Chem. B* **2004**, *108*, 7534–7537.
(15) Gao, P. X.; Ding, Y.; Wang, Z. L. *Nano Lett.* **2003**, *3* (9), 1315–1320.
(16) Gundiah, G.; Deepak, F. L.; Govindaraj, A.; Rao, C. N. R. *Top. Catal.* **2003**, *24* (No. 1−4), 137–146.
(17) Wang, J.; Sha, J.; Yang, Q.; Ma, X.; Zhang, H.; Yu, J.; Yang, D. *Mater. Lett.* **2005**, *59*, 2710–2714.
(18) Lim, Y. S.; Park, J. W.; Kim, M. S.; Kim, J. *Appl. Surf. Sci.* **2006**, *253*, 1601–1605.
(19) Gao, P. X.; Lao, C. S.; Ding, Y.; Wang, Z. L. *Adv. Funct. Mater.* **2006**, *16*, 53–63.
(20) Huang, M.; Mao, S.; Feick, H.; Yan, H. Q.; Wu, Y. Y.; Kind, H.; Weber, E.; Russo, R.; Yang, P. *Science* **2001**, *292*, 1897–1899.
(21) Pan, Z. W.; Dai, Z. R.; Wang, Z. L. *Science* **2001**, *291*, 1947–1949.
(22) Gao, P. X.; Wang, Z. L. *J. Appl. Phys.* **2005**, *97*, 044304–044311.
(23) Kim, Y. Y.; Ahn, C. H.; Kang, S. W.; Kong, B. H.; Mohanta, S. K.; Cho, H. K.; Lee, J. Y.; Kim, H. S. *J. Mater. Sci.: Mater. Electron.* **2008**, *19*, 749–754.
(24) Yu, Z.; Aceves-Mijares, M.; Luna-Lopez, A.; Du, J.; Bian, D. *Nanotechnology* **2006**, *19*, 4962–4965.
(25) Piscopiello, E.; Tapfer, L.; Antisari, M. V.; Paiano, P.; Prete, P.; Lovergine, N. *Phys. Rev. B* **2008**, *78*, 035305(1)–035305(7).
(26) Rao, C. N. R.; Gundiah, G.; Deepak, F. L.; Govindaraja, A.; Cheetham, A. K. *J. Mater. Chem.* **2004**, *14*, 440–450.
(27) Rao, C. N. R.; Deepak, F. L.; Gundiah, G.; Govindaraj, A. *Prog. Solid State Chem.* **2003**, *31*, 5–147.
(28) Pilania, G.; Sadowski, T.; Ramprasad, R. *J. Phys. Chem. C* **2009**, *113*, 1863–1871.
(29) Doll, J. D.; Pilania, G.; Ramprasad, R.; Papadimitrakopoulos, F. *Nano Lett.* **2010**, *10*, 680–685.
(30) Gay, R. R.; Nodine, M. H.; Henrich, V. E.; Zeiger, H. J.; Solomon, E. I. *J. Am. Chem. Soc.* **1980**, *102*, 6752–6761.
(31) Huang, M. H.; Wu, Y.; Feick, H.; Tran, N.; Weber, E.; Yang, P. *Adv. Mater.* **2001**, *13*, 113–116.
(32) Yanagida, T.; Marcu, A.; Matsui, H.; Nagashima, K.; Oka, K.; Yokota, K.; Taniguchi, M.; Kawai, T. *J. Phys. Chem. C* **2008**, *112*, 18923–18926.